ISSN 0001-4370, Oceanology, 2006, Vol. 46, No. 6, pp. 772–783. © Pleiades Publishing, Inc., 2006.
Original Russian Text © G.G. Panteleev, M.N. Koshlyakov, E.G. Morozov, R.Yu. Tarakanov, A.Yu. Goldin, A.Yu. Shcherbina, M. Ikeda, 2006, published in Okeanologiya, 2006, Vol. 46, No.6, pp. 821–833.

MARINE PHYSICS

Numerical Modeling of Currents in the Drake Passage with Assimilation of the Experimental Data of 2003

G. G. Panteleev[a,b], M. N. Koshlyakov[a], E. G. Morozov[a], R. Yu. Tarakanov[a], A. Yu. Goldin[a], A. Yu. Shcherbina[c], and M. Ikeda[a]

[a] *Shirshov Institute of Oceanology, Russian Academy of Sciences, Moscow, Russia*
[b] *International Arctic Research Center, Fairbanks, Alaska, USA*
[c] *Woods Hole Oceanographic Institution, Woods Hole, Massachusetts, USA*
[d] *Hokkaido University, Sapporo, Japan*

Received May 15, 2006

Abstract—Computation of ocean currents in the Drake Passage is carried out with variational assimilation of the data of the hydrographical section across the Drake Passage carried out on December 11–15, 2003, and other data. A stream-eddy structure of the easterly Antarctic Circumpolar Current and a westerly current on the Antarctic Slope are obtained. Water transports by the different current field components and the integral transport across the Drake Passage are estimated. The necessity of direct current measurements in the Drake Passage for a correct estimate of the transport is confirmed.

DOI: 10.1134/S0001437006060026

INTRODUCTION

By the end of the 1970s, as a result of the studies of oceanic currents in the Drake Passage, which have continued over more than one decade, a multijet and strongly nonstationary character of the Antarctic Circumpolar Current (ACC) was finally established. It was manifested in the meridional displacements of individual jets, their meandering, and the formation of cyclonic and anticyclonic eddies of synoptic scale. In addition, it was found that the current velocities at the ocean bottom are usually equal to a few centimeters per second [12, 20], which leads to significant errors in the calculation of the geostrophic velocity and transport by currents using the dynamical method and the reference surface either coinciding with the bottom or located above the bottom. It follows from this that the observations over the section across the strait should satisfy two main conditions for the adequate reflection of the structure of the currents:

(1) Hydrophysical (CTD) measurements should be made to the bottom of the ocean and the distances between the CTD stations should be small enough to resolve individual jets, eddies, fronts, and slope currents.

(2) CTD measurements should be accompanied by direct measurements of currents at least at one level with a resolution in the direction across the strait not less than that of the CTD measurements.

Judging from the known publications, the requirements mentioned above are more or less satisfied by the measurements over four sections across the strait from Cape Horn to Livingston Island (see Fig. 1) carried out in 1975 and 1979 onboard the USA vessels *Melville* and *Atlantis II* and the Chilean vessel *Yelcho* [12, 20]. During these expeditions, direct measurements of currents were performed at depths of 1000–3500 m with chains of subsurface moorings oriented across the strait. It should be noted, however, that the distances between the moorings were notably greater than the distances between the CTD stations over the sections. As to the studies over the section from the Burdwood Bank south of the Falkland Islands to Elephant Island in the eastern part of the strait, which have been regularly performed from 1993 by British and Spanish oceanographers, one can judge from [6] and [8] that the direct measurements of currents using a lowered acoustic Doppler current profiler (LADCP) over this section were not successful at least before 2001. The aforesaid points to the necessity of performing further detailed hydrophysical observations in the Drake Passage, which include direct measurements of currents.

INITIAL DATA AND METHOD OF CURRENTS CALCULATION

The calculation of currents in the Drake Passage described in this paper was performed using the method of variational data assimilation in the numerical model of oceanic circulation. The following data were used as the initial data:

(1)The data of CTD profiling to the bottom of the ocean at 25 stations of the hydrographic section across the Drake Passage performed from R/V *Akademik Sergei Vavilov* of the Shirshov Institute of Oceanology, RAS, on December 11–15, 2003 (Fig. 1) [3]. The corresponding temperature and salinity values were smoothed over the depth and interpolated to 45 model

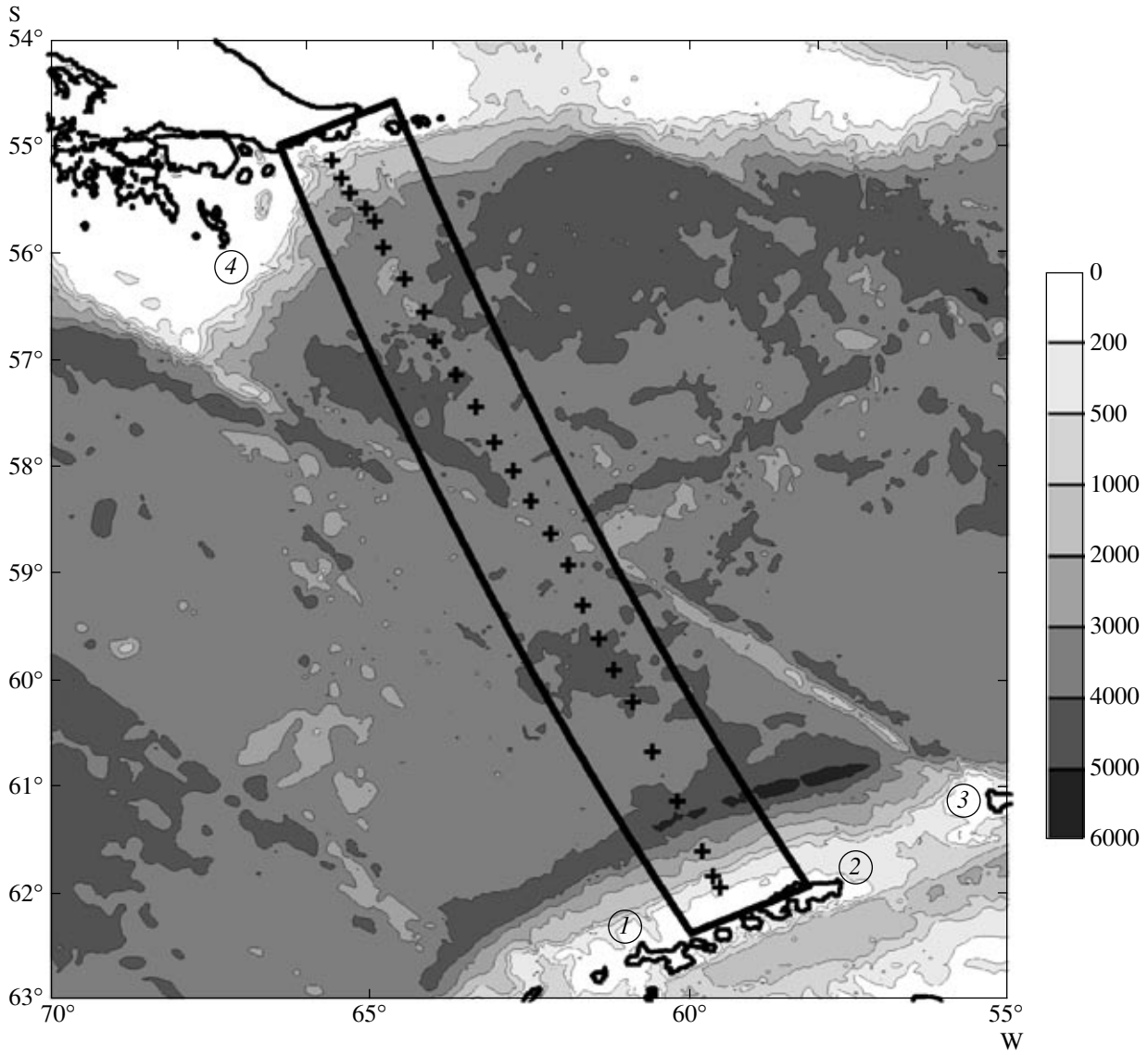

Fig. 1. Locations of the CTD/LADCP stations over the section across the Drake Passage performed by R/V *Akademik Sergei Vavilov* from December 11 (southern edge of the section) to December 15, 2003, and the region of the calculations of the currents. The depth scale in meters is shown on the right. *1*—Livingston Island, *2*—King George Island, *3*—Elephant Island, *4*—Cape Horn.

levels. The root-mean-square (r.m.s.) errors in the fields of the temperature and salinity were estimated by analyzing the variability of these characteristics along the section, and it was assumed that they vary from 1°C and 0.1 psu at the surface of the ocean to 0.2 °C and 0.01 psu at a depth of 4 km.

(2) The continuous SADCP (shipborne acoustic Doppler current profiler) data along the section of 2003 in the layer between 25 and 300 m. These data were smoothed over the section with a scale of 60 km and were also smoothed over the depth. The depth-dependent r.m.s. of these data was assumed to be equal to 25% of the mean square variability (MSV) of the corresponding values of the velocity along the section. Owing to the fact that the vectors of the SADCP velocity were unnaturally directed to the continental slope in the southern 50-km interval of the section (see Fig. 7 below), the components of these vectors parallel to the section were not taken into account in the calculations.

(3) The LADCP data of velocity measurements over the entire depth of the ocean at the stations in 2003. Similar to the CTD data, these data were smoothed over the depth and interpolated to 45 model levels. Owing to the complicated processing of LADCP data, which includes, in particular, accounting for the velocities of the ship's drift and the lowering of the CTD/LADCP profilers [18], the r.m.s. of these data was assumed to be equal to 2 cm/s plus 50% of the MSV of the corresponding velocities along the section at a given depth.

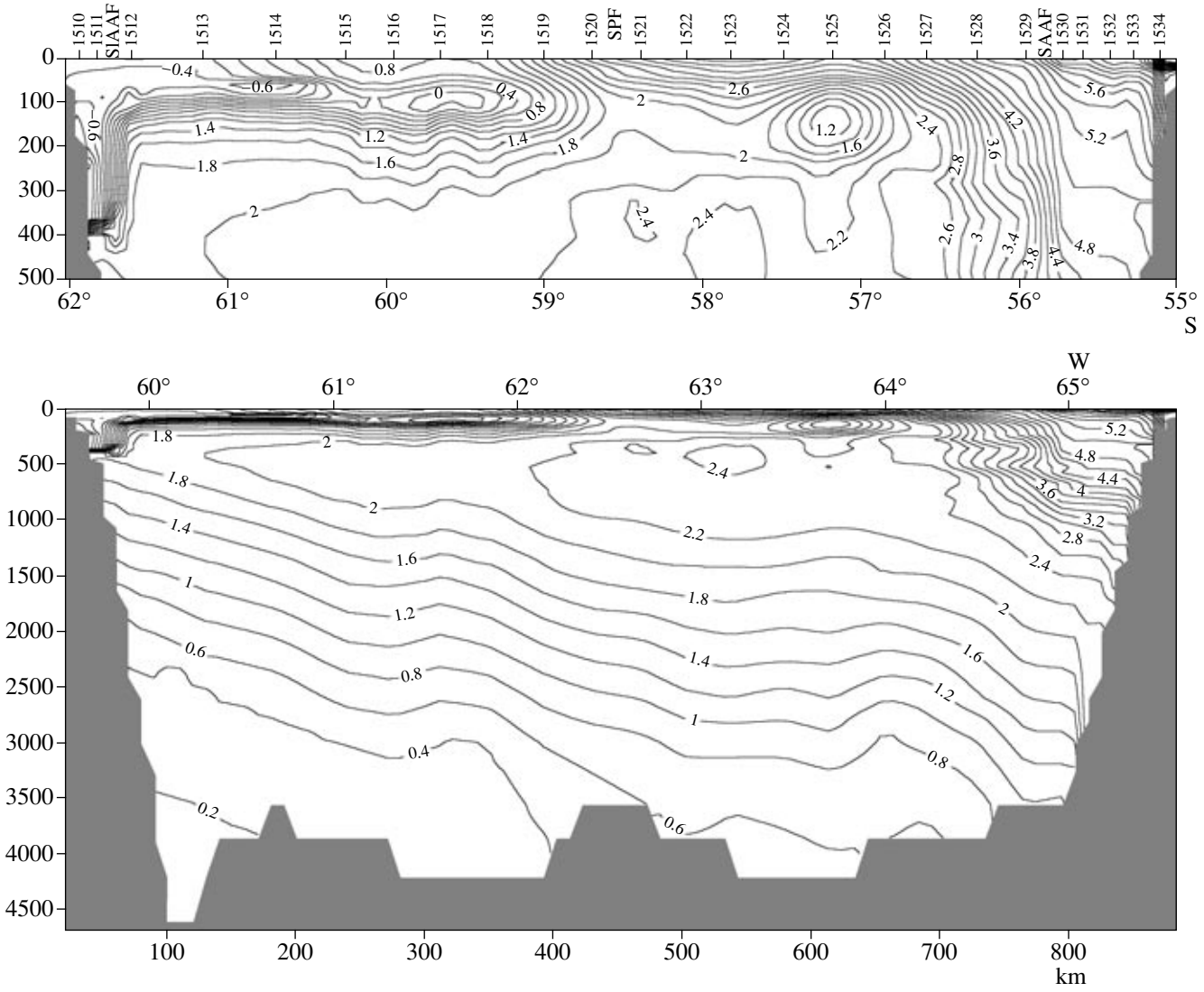

Fig. 2. Potential temperature (°C) over the section across the Drake Passage on December 11–15, 2003. The SlAAF, SPF, and SAAF are the Slope Antarctic Front, the South Polar Front, and the Sub-Antarctic Front, respectively. The locations and numbers of the CTD stations are shown above. The depth in meters is shown on the left.

(4) The results of the calculation of geostrophic currents at the ocean surface (Fig. 1) available at http://www.jason.oceanobs.com prepared at the Department of Satellite Oceanography of the French CLS (Collecte Localisation Satelittes) Agency based on the altimetry data of the *ERS-1, ERS-2*, and *TOPEX/Poseidon* satellites [7]. These results were averaged over three dates: December 10, 13, and 17, 2003. Similarly to the SADCP data, the r.m.s. of the obtained velocities was assumed to be equal to 2 cm/s plus 25% of the MSV of these values within the study region.

(5) The densities of the momentum flux (tangential wind stress) and the fluxes of heat and salt at the ocean surface in the study region (Fig. 1) obtained from a reanalysis of meteorological data available from the NCEP/NCAR array at (http://www.cdc.noaa.gov/cdc/reanalysis/index.html). These values were averaged over a period of one week, which includes the time of performing the 2003 section. The r.m.s. of these data was assumed to be equal to 40% of the MSV of the densities of the corresponding fluxes within the study region.

According to the aforesaid, the problem of the calculation of currents in the Drake Passage was solved by minimizing the functional J (cost function, which is given below) over a set of solutions of the numerical model of the ocean circulation. A nonstationary and nonlinear model based on the traditional primitive equations of motion with hydrostatic and Boussinesq approximations [4] was used as such a model. A prototype of this model is the Ocean Parallelized Ocean General Circulation Model (OPA OGCM) [10]. A modification of the OPA OGCM developed in [4] consists mainly of an implicit description of the Coriolis

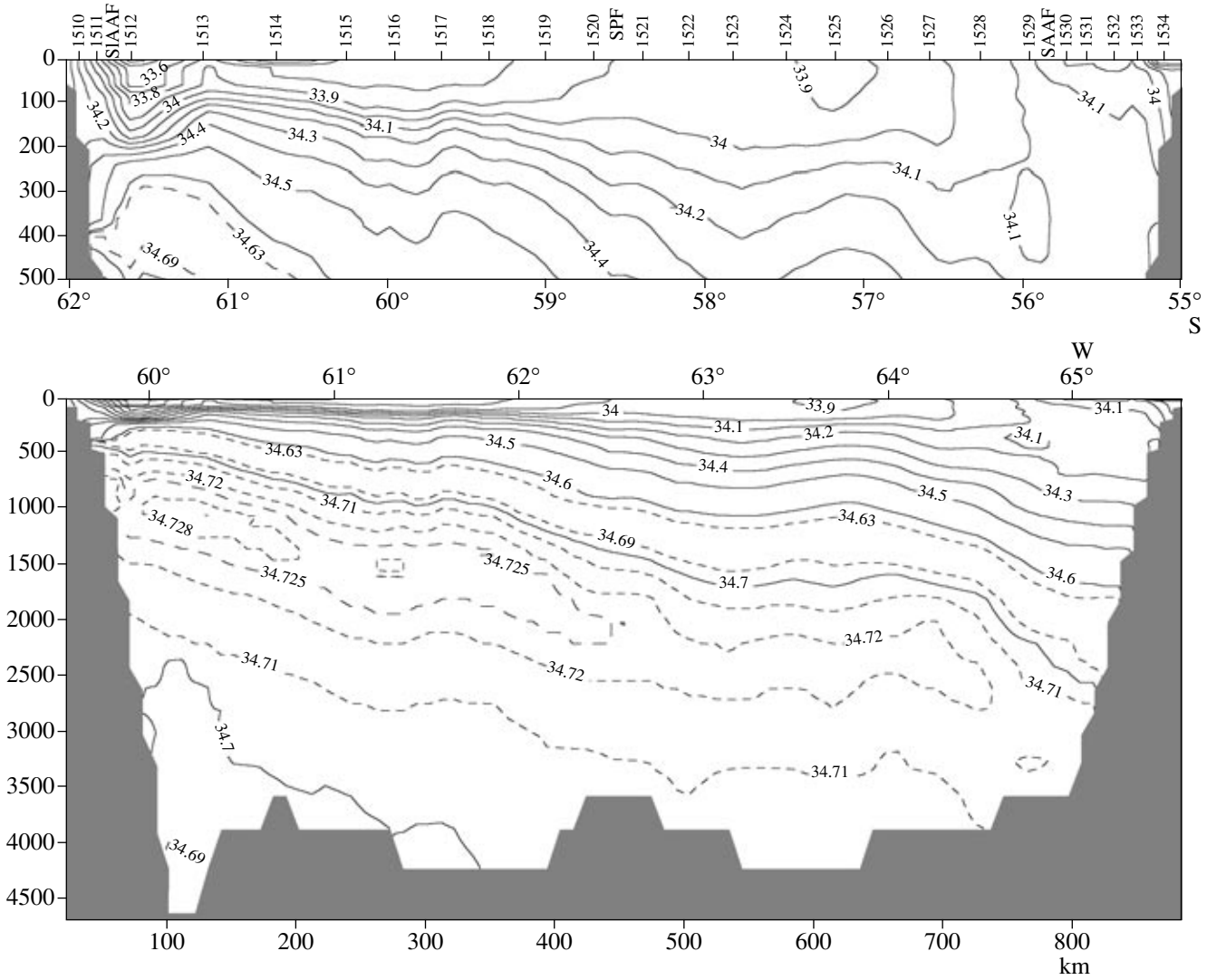

Fig. 3. Salinity (psu) over the section across the Drake Passage on December 11–15, 2003. See Fig. 2 for other notations.

acceleration and "fast" processes, which include surface gravity waves, and a semi-implicit description of "slow" processes, which include internal gravity waves and adjustment of the density field to the perturbations of the ocean level.

Model [4] allows one to restore the evolution of the fields of the temperature, salinity, current velocity, and level surface within an arbitrary region of the ocean. The initial distributions of the temperature and salinity $\mathbf{C} = (T, S)$, the horizontal component of the current velocity $\mathbf{u}$, and the perturbations of the ocean level ζ within the region considered, as well as the linearly time-dependent distributions of $\mathbf{C} = (T, S)$ and the velocity component $\mathbf{u}_n$ normal to the boundary at the open (oceanic) boundaries Γ_1 of this region, and the distributions of the density fluxes of heat, salt $\mathbf{B}$, and momentum $\boldsymbol{\tau}$ at the ocean surface Γ_2 are used as free parameters ("control vectors" of the $\mathbf{Y}$ model) whose specifying minimizes the cost function J (here, $\mathbf{Y} = [(\mathbf{C}, \mathbf{u}, \zeta)_{t=0}, (\mathbf{u}_n, \mathbf{C})_{\Gamma_1}, (\mathbf{B}, \boldsymbol{\tau})_{\Gamma_2}]$. Detailed descriptions of the equations of the model, the numerical scheme, and the approximation of the boundary conditions are given in [4].

The following functional was taken as the cost function:

$$J = J_1 + J_2,$$

$$J_1 = (\Omega T_m)^{-1} \times \int\limits_{\Omega, T_0} \left[W_{\mathbf{C}}^{-1} (\mathbf{C} - \mathbf{C}^*)^2 + W_{\mathbf{u}}^{-1} (\mathbf{u} - \mathbf{u}^*)^2 \right] d\omega dt$$

$$+ (S_0 T_m)^{-1} \int\limits_{z=0} \left[W_{\boldsymbol{\tau}}^{-1} (\boldsymbol{\tau} - \boldsymbol{\tau}^*)^2 + W_{\mathbf{B}}^{-1} (\mathbf{B} - \mathbf{B}^*)^2 \right] ds dt,$$

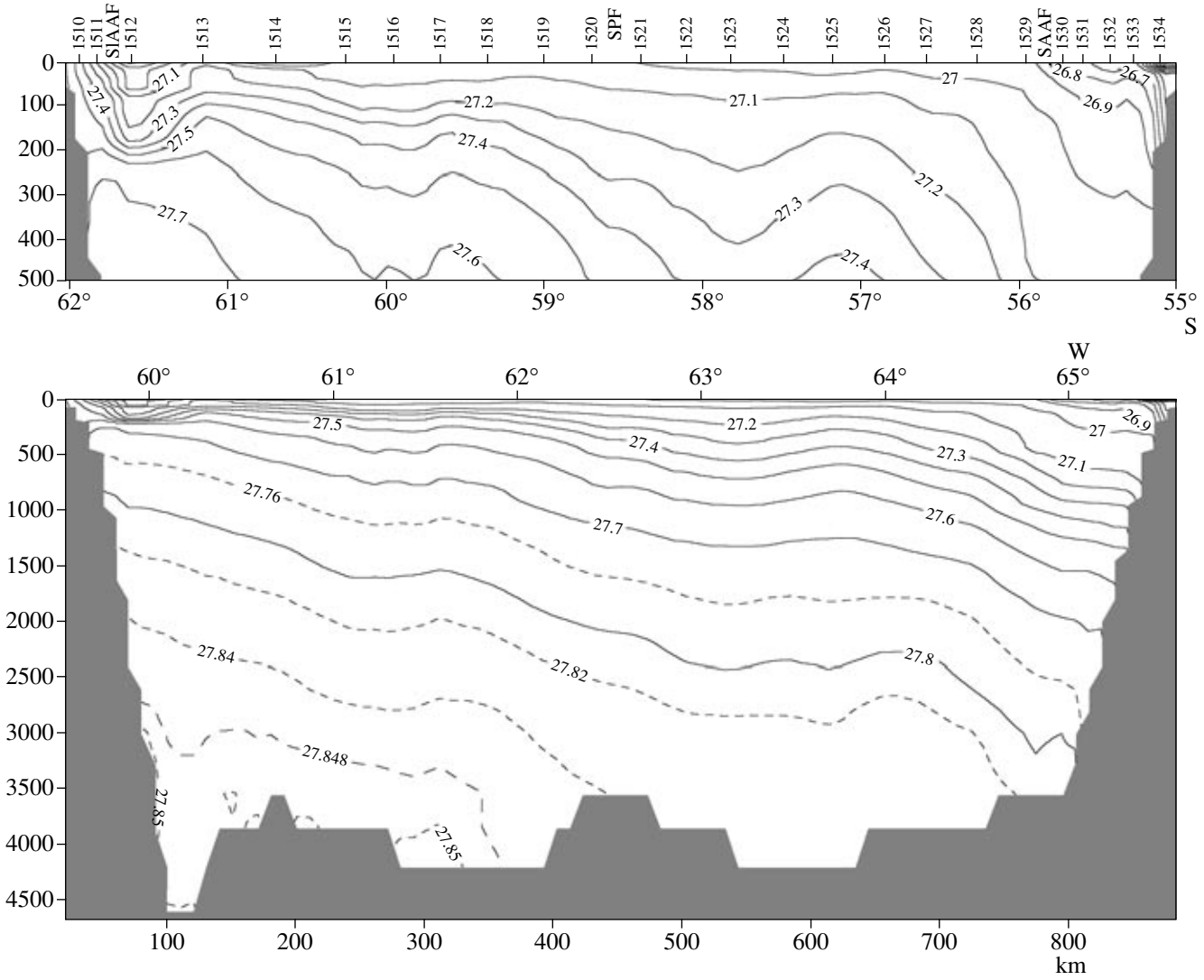

Fig. 4. Potential density σ_θ over the section across the Drake Passage on December 11–15, 2003. See Fig. 2 for other notations.

$$J_2 = (\Omega T_m)^{-1}$$

$$\times \int\limits_{\Omega, T_0} \Big[W^{-1}_{\mathbf{C},s}(\Delta \mathbf{C})^2 + W^{-1}_{\mathbf{u},s}(\Delta \mathbf{u})^2$$

$$+ W^{-1}_{\mathbf{C},tt}\mathbf{C}^2_{tt} + W^{-1}_{\mathbf{u},tt}\mathbf{u}^2_{tt}\Big] d\omega dt + (S_0 T_m)^{-1}$$

$$\times \int\limits_{z=0} \Big[W^{-1}_{\zeta,s}(\Delta\zeta)^2 + W^{-1}_{\tau,s}(\Delta\boldsymbol{\tau})^2 + W^{-1}_{\mathbf{B},s}(\Delta \mathbf{B})^2$$

$$+ W^{-1}_{\zeta,tt}\zeta^2_{tt}\Big] ds dt.$$

Here, the asterisk denotes the data of observations; Ω and S_0 are the volume of the calculation region (Fig. 1) and its area at the ocean surface, respectively; T_m is the model time interval; $W_{\mathbf{C}}$, $W_{\mathbf{u}}$, $W_{\mathbf{B}}$, and W_τ are the variances of the errors of the corresponding data; and $W_{\mathbf{C},s}$, $W_{\mathbf{u},s}$, $W_{\zeta,s}$, $W_{\mathbf{B},s}$, $W_{\tau,s}$, $W_{\mathbf{C},tt}$, $W_{\mathbf{u},tt}$ and $W_{\zeta,tt}$ are the variances of the errors in the estimates of the corresponding Laplacians and second derivatives with respect to time. The other notations were explained above.

A minimization of the functional J approximates the solution of the problem to the data of observations and suppresses high-frequency noises in the calculated fields. The methods of specifying the values of $W_{\mathbf{C}}$, $W_{\mathbf{u}}$, $W_{\mathbf{B}}$, and W_τ were described above. Inverse weights of the smoothing terms of the cost function were estimated in the following manner:

$$W_{C,s} = \mathbf{C}^2_s/L^4_C, \quad W_{\mathbf{u},s} = V^2_s/L^4_u, \quad W_{\zeta,s} = \zeta^2_s/L^4_u,$$

$$W_{\tau,s} = \tau^2_s/L^4_\tau, \quad W_{\mathbf{B},s} = \mathbf{B}^2_s/L^4_C, \quad W_{\mathbf{C},tt} = \mathbf{C}^2_t/T^4_{\text{var}},$$

$$W_{\mathbf{u},tt} = \mathbf{u}^2_t/T^4_{\text{var}}, \quad W_{\zeta,tt} = \zeta^2_t/T^4_{\text{var}}.$$

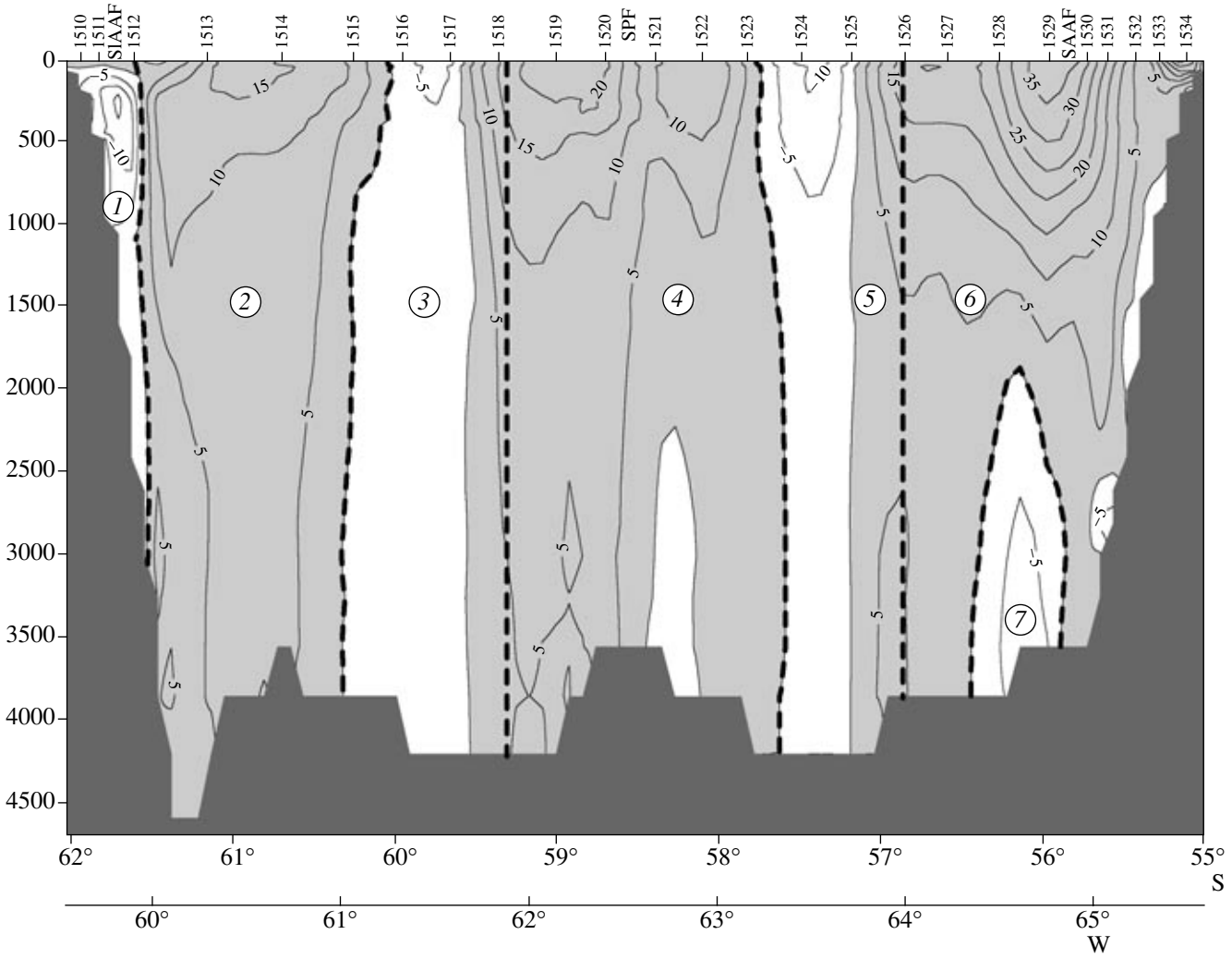

Fig. 5. Component of velocity (cm/s) normal to the section across the Drake Passage. The shaded regions of the section with positive velocity values correspond to the currents with an eastern component. The heavy dashed lines and the numerals in the circles show the boundaries and numbers of individual structural elements of the current field (see the table). See Fig. 2 for other notations.

The dispersions $\mathbf{C}_s^2$, $\boldsymbol{\tau}_s^2$, $\mathbf{B}_s^2$, $\mathbf{C}_t^2$, $\mathbf{u}_t^2$ and ζ_t^2 of the spatial and temporal variability of the corresponding fields were estimated from the data of observations. It was assumed that $V_s = 30$ cm/s and $\zeta_s = 50$ cm. According to the data of observations, the following values were specified for the spatial and temporal scales of the fields studied: $L_C = L_u = 100$ km, $L_\tau = 500$ km, and $T_{\text{var}} = 30$ days.

Traditionally, the solution of the problem was found using the method of successive approximation. In the first approximation, the distributions of the model variables maximally close to the data of observations were taken as the control vector. The method of specifying the control vector in the first approximation, as well as all the mathematical details of minimizing the cost function J, are described in detail in [4]. The calculation was performed in the spherical domain shown in Fig. 1, which spreads to the bottom. Its longitudinal axis is rotated by 19° with respect to the meridian. The time of the calculation was equal to six days, which included the time of performing the section in 2003. The resolution of the calculation was equal to 0.09° and 0.25° in the directions along and across the section, respectively, at 45 vertical levels. The time step was equal to 0.05 day. The dimension of the grid area was $11 \times 91 \times 45 \times 120 = 5\,405\,400$ spatiotemporal points. The size of the control vector was equal to 163 602 points. The bottom topography was restored from the ETOPO05 data.

In the next section, we present the distributions of the oceanographic characteristics on December 13, 2003, obtained from the calculations. However, taking into account that, during the model time interval equal to six days, these distributions varied only slightly and the meteorological and altimetric information assimilated in the calculation correspond to weekly averaging over time, the distributions obtained can be interpreted

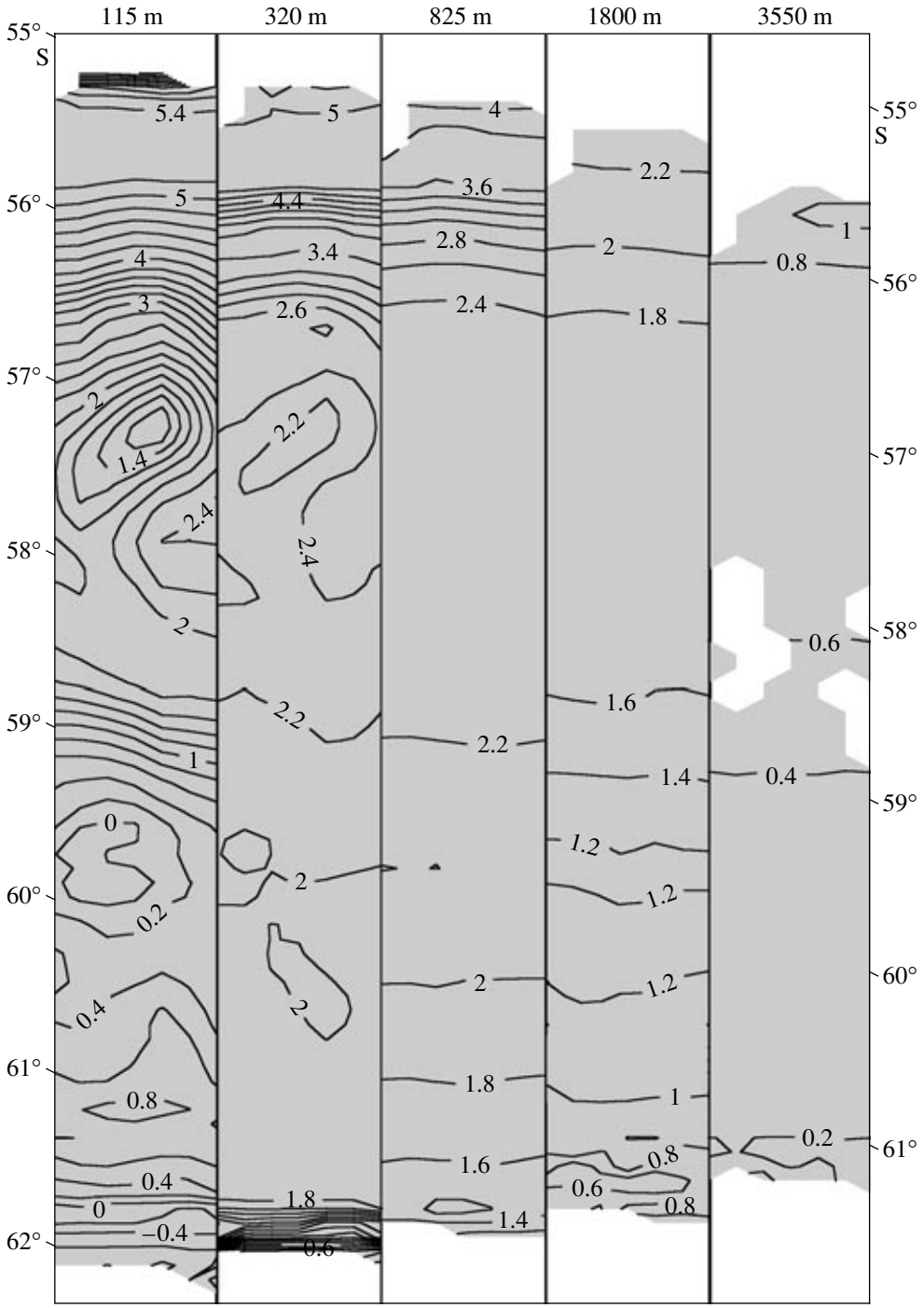

Fig. 6. Potential temperature (°C) at depths of 115, 320, 825, 1800, and 3550 m in the calculation region (Fig. 1). The tics and the numerals at the left and right limits of the figure show the southern latitudes.

as the mean distributions characteristic of the period from December 10 to 17, 2003.

RESULTS OF THE CALCULATION

The distributions of the oceanographic characteristics restored as a result of the calculations described in the previous section and the corresponding velocity fields are shown in Figs. 2–7 and presented in the table. The obtained distributions of the potential temperature θ, salinity S, and potential density σ_θ in the plane of the section in 2003 (Figs. 2–4) are close to the initial ones (observed); therefore, the latter are not shown. The locations of the Sub-Antarctic (SAAF), Southern Polar (SPF), and Slope Antarctic (SlAAF) fronts in Figs. 2–4 are traditionally determined as the transition of the sur-

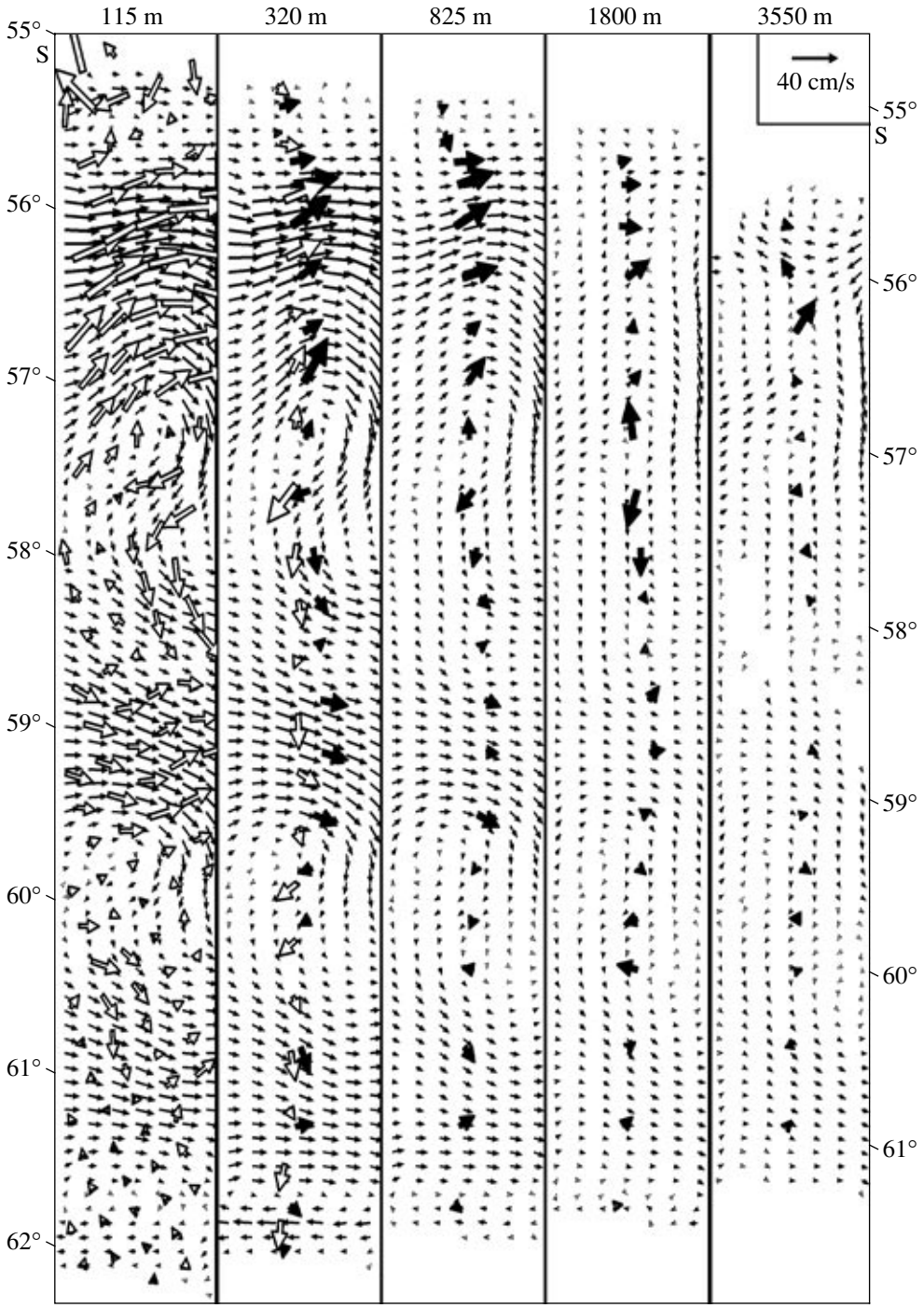

Fig. 7. Distribution of the horizontal component of velocity at individual levels in the calculation region (Fig. 1). The thick white arrows in the chart of the 115-m depth show the velocities at the surface of the ocean obtained from the data of satellite altimetric observations. The thick white arrows in the chart of the 320-m level show the velocities measured by SADCP at a depth of 300 m. The thick black arrows in the charts for depths of 320, 825, 1800, and 3550 m are the velocity vectors at these depths from the LADCP data. The velocity scale is shown in the upper right-hand part of the figure. See Fig. 6 for other notations.

face minimum of S into the intermediate minimum in the northward direction north of the northern boundary of the subsurface minimum of θ, which is continuous by latitude, and the northern boundary of the cold mixed subsurface layer of increased thickness. The oceanic zone north of the SAAF is called the Sub-Antarctic zone (SAAZ), the zone between the SAAF and SPF is the Southern Polar Frontal zone (SPFZ), the zone

Water transports in individual structural elements of the current field (Fig. 5)

Structural element	Number in Fig. 5	Transport, 10^6, m^3/s
Slope Antarctic Current	1	–3.3
South Antarctic Current	2	+39.8
Cyclonic eddy south of the South Polar Current	3	6.1
South Polar Current	4	+42.0
Cyclonic eddy south of the Sub-Antarctic Current	5	6.5
Sub-Antarctic Current	6	+ 46.4
Countercurrent below the Sub-Antarctic Current	7	–3.3

Note: The positive and the negative transports denote the easterly and the westerly currents, respectively. For two cyclonic eddies with a zero integral transport across the strait, the transport is given for one direction only.

between the SPF and SlAAF is the Antarctic zone (AAZ), and the zone south of the SlAAF is the Slope Antarctic zone (SlAAZ).

All the main water masses of the Antarctic are well seen in Figs. 2–4. In the AAZ and SlAAZ, the upper layer of the ocean is occupied by the fresh and cold Antarctic Surface Water (AASurW) with indications of an admixture of even cooler and more saline Antarctic Shelf Water (AAShW) in the SlAAZ. The relatively poorly saline Antarctic Intermediate Water (AAIW) is located in the upper layer of the SPFZ, which descends in the SAAZ to the depths of 500–1000 m. In the SAAZ, the upper layer is occupied by the Sub-Antarctic Mode Water (SAAMW) with a quasi-pycnostad at depths of 100–500 m. The Upper Circumpolar Deep Water (UCDW) is located south of the SAAF immediately below the waters mentioned above with an intermediate maximum of θ; the Lower Circumpolar Deep Water (LCDW) with an intermediate maximum of *S* at depths of 1000–3000 m is located below this water mass. Finally, the Circumpolar Bottom Water (CBW) is located below the LCDW and occupies the entire deep ocean layer down to the bottom in the zone north of 60° S. The CBW can be considered as the lowest layer of Circumpolar Deep Water. In the Southwest Atlantic, owing to its deep location, it is not renewed by the North Atlantic Deep Water in the course of its motion around the Antarctic continent in the ACC field [2]. In the zone south of 60° S, the bottom layer of the ocean under the CBW is occupied by the Antarctic Bottom Water (AABW), which is cooler and less saline than the CBW.

The results of the calculation of the currents presented in Figs. 5 and 7 make it possible to distinguish individual structural elements of the velocity field. The boundaries between these elements are shown in Fig. 5, while the water transports are given in the table. A comparison of Figs. 5 and 7 allows us to understand the interpretation of the velocity field obtained by us and reflected in the names of the structural elements of the field in the table. According to the table, the jets of the ACC corresponding to the SAAF, SPF, and the middle of the AAZ, we call the Sub-Antarctic, the South Polar, and the Southern Antarctic currents (SAAC, SPC, and SthAAC).

The division of the ACC into the SAAC, SPC, and SthAAC became finally clear from the middle of the 1990s [1, 14]. According to the data we obtained, the width of the SAAC, the SPC, and the SthAAC during the period of the observations was approximately the same, being approximately equal to 180 km (Fig. 5). The maximal velocity of the SAAC in the upper layer of the ocean exceeded by 1.5 and 2 times the maximal velocity of the SPC and the SthAAC, respectively (Fig. 5). Meanwhile, the water transports by these three currents appeared to be close (table). The author of [1] analyzed the data of 13 sections of R/V *Eltanin* and other vessels across the ACC in different parts of the Antarctic ring. The mean values of the geostrophic transports over the Antarctic ring for the SAAC, the SPC, and the SthAAC calculated using the dynamical method relative to the bottom of the ocean were equal to 56×10^6, 37×10^6, and 19×10^6 m^3/s, respectively. The difference between the ratio of these values and the ratio we obtained for the SAAC, the SPC, and the SthAAC (table) is mainly explained be the fact that the more southern location of the ACC jet is accompanied by a lesser decrease of velocity with depth. Indeed, according to our results (Fig. 5), both the SPC and the SthAAC are characterized by an equivalent barotropic structure with the conservation of the easterly direction of the current down to the ocean bottom. However, the average velocity of the SthAAC at the bottom is greater than the velocity of the SPC. At the same time, the SAAC is characterized by the existence of acountercurrent in the bottom layer of the ocean. It follows from this that the calculation of the geostrophic current velocity using the dynamical method relative to the bottom should lead to an increase in the transport of the SAAC and to a decrease in the transports of the SPT and, especially, of the SthAAC.

The distributions of θ over the section (Fig. 2) and at a depth of 115 m (Fig. 6) clearly demonstrate that the well manifested eddies located immediately south of the SPC and south of the SAAC (structural elements 3 and 5 in the table and Fig. 5) were, correspondingly, the results of the formation and further separation of cyclonic meanders of the SAAC and the SPC. It is not excluded that, in one or in both of these cases, longitudinal splitting of the current occurred before the meandering; thus, only the northern part of the current separated. This suggestion is confirmed by the moderate values of the negative anomalies of θ in the upper layer of the ocean at the centers of the cyclones described here (Fig. 2) and their small internal transports (table).

The full size of the SPC and SAAC cyclonic eddies was equal to 100–120 km (Figs. 5, 7). The interaction of these eddies with the jet of the ACC located immediately north of them resulted in an eddy structure that is nonsymmetric with respect to their zonal axes. The easterly currents in the northern parts of these eddies were significantly stronger and narrower than the compensating westerly currents in their southern parts (Fig. 5). It is also seen well from Figs. 5 and 7 that both of the cyclones described here, as well as the jets of the ACC that formed them, had an equivalent–barotropic structure with a velocity of the near-bottom currents of a few cm/s. One can conclude that the results obtained during the expedition in 2003 generally correlate with the concepts of the high intensity of the process of synoptic eddy formation in the Drake Passage (for example, [15, 17]), which has been generally accepted by the present time. Meanwhile, they showed that this process is related to the instability not only of the SAAC and the SPC but also of the SthAAC.

As seen from Figs. 5 and 7, the calculations showed the existence of a deep westerly countercurrent under the axial part of the SAAC with a velocity near the bottom exceeding 5 cm/s (structural element 7 in Fig. 5 and in the table). It is remarkable that the measurements of the currents in the Drake Passage carried out in March–October 1975, which were mentioned in the Introduction, are in good agreement with our results. They showed the existence of a stable westerly current with a mean velocity of approximately 2 cm/s at a depth of 3200 m in the zone corresponding to the southern part of the SAAC [5]. Thus, one can suppose that the countercurrent described here is a quasi-permanent element of the field of currents in the Drake Passage.

According to the calculations, during the period of the observations, the westerly Slope Antarctic Current (SlAAC) (element 1 in Fig. 5 and in the table) spread to a depth of 3100 m and was approximately 50 km wide in its upper part and approximately 10 km wide at a depth of 2000 m. It was characterized by a maximal velocity equal to 15 cm/s at a depth of 300 m. The result obtained related to the direction of the current agrees well with the results of the long-term measurements of the currents at depths of 500 and 2700 m carried out in January 1979–February 1980 at several moorings over the Antarctic slope north of Livingston Island (Fig. 1) [13]. As a result of these measurements at both depths, the authors found stable currents directed to the west-southwest along the depth contours with mean velocities of 4 cm/s at a depth of 500 m and 9 cm/s at 2700 m.

A comparison of Figs. 2, 3, 4, and 5 shows that the slope modification of the AAIW occupied the upper part of the SlAAC down to depths of 300–400 m, which differed from the AAIW located north of it by a lower temperature, slightly higher salinity, and a significantly greater thickness of its layer. According to the historical and present-day data of the hydrophysical observations performed in the northwestern part of the Weddell Sea and in the Drake Passage, which were described in [9, 16, 19], one can suppose with a high degree of confidence that this water is a result of mixing between the UCDW in the Drake Passage and the cold water of the Bransfield Strait, which is transported to the Drake Passage through the Loper Strait (500 m deep) between King George and Elephant islands (Fig. 1). In its turn, the water of the Bransfield Strait is formed by mixing between the AAShW formed as a result of the winter convection over the northwestern shelf of the Antarctic Peninsula with the UCDW transported to the Weddell Sea from the ACC zone in the northeast [16, 19]. The flow of the cold and heavy water of the Bransfield Strait from the south to the zone of the upper part of the slope of the South Shetland Islands forms a pressure gradient in this zone directed to the south, which increases its value from zero at the ocean surface to the maximum at the lower boundary of the layer to which this water spreads. This effect corresponds to the westerly geostrophic current with a maximum velocity at a depth of 300–400 m (Figs. 5, 7).

The physical origin of the deep part of the SlAAC (below 1000 m) (Fig. 5) is similar to the origin of the upper part of this current described above with the single difference being that other water masses also take part in the formation of the deep part of the SlAAC. According to [11, 13, 19], the cold and freshened deep water of the Weddell Sea (AABW, according to an alternative terminology) flows to the southern part of the Scotia Sea via deep passages east and west of the South Orkney Islands at depths below 1200 m. Later, this water mixes with the LCDW and the CDW in the ACC zone. The water mass formed as a result of this mixing flows to the west along the northern slope of the South Orkney and South Shetland islands owing to the excess of its density over the density of the adjacent waters in the north (Fig. 4). According to [11, 13], the westerly current over the northern slope of the South Shetland Islands spreads only to the greatest depths of the ocean including the deep trench at 61°20′ S (Figs. 2–5). Since, in our calculations, we did not obtain this deep part of the SlAAC (Fig. 5), it is likely that the measurements in the southern part of the section studied here were made with a resolution that was not sufficient to distinguish this effect.

According to the results of the calculations (Fig. 5, table), the total water transport via the Drake Passage was equal to 121.6×10^6 m^3/s in the eastern direction. The measurements of the integral transport via the Drake Passage from Cape Horn to Livingston Island (Fig. 1) performed from February 1979 to January 1980, which included joint measurements of the currents, pressure, and temperature with a chain of moorings oriented across the strait, accompanied by pressure measurements with bottom gauges located at the continental slopes on both sides of the strait, resulted in an annual mean value of the transport equal to 134×10^6 m^3/s [21]. These measurements also distinguished a notable seasonal variability of the transport with a maximum in

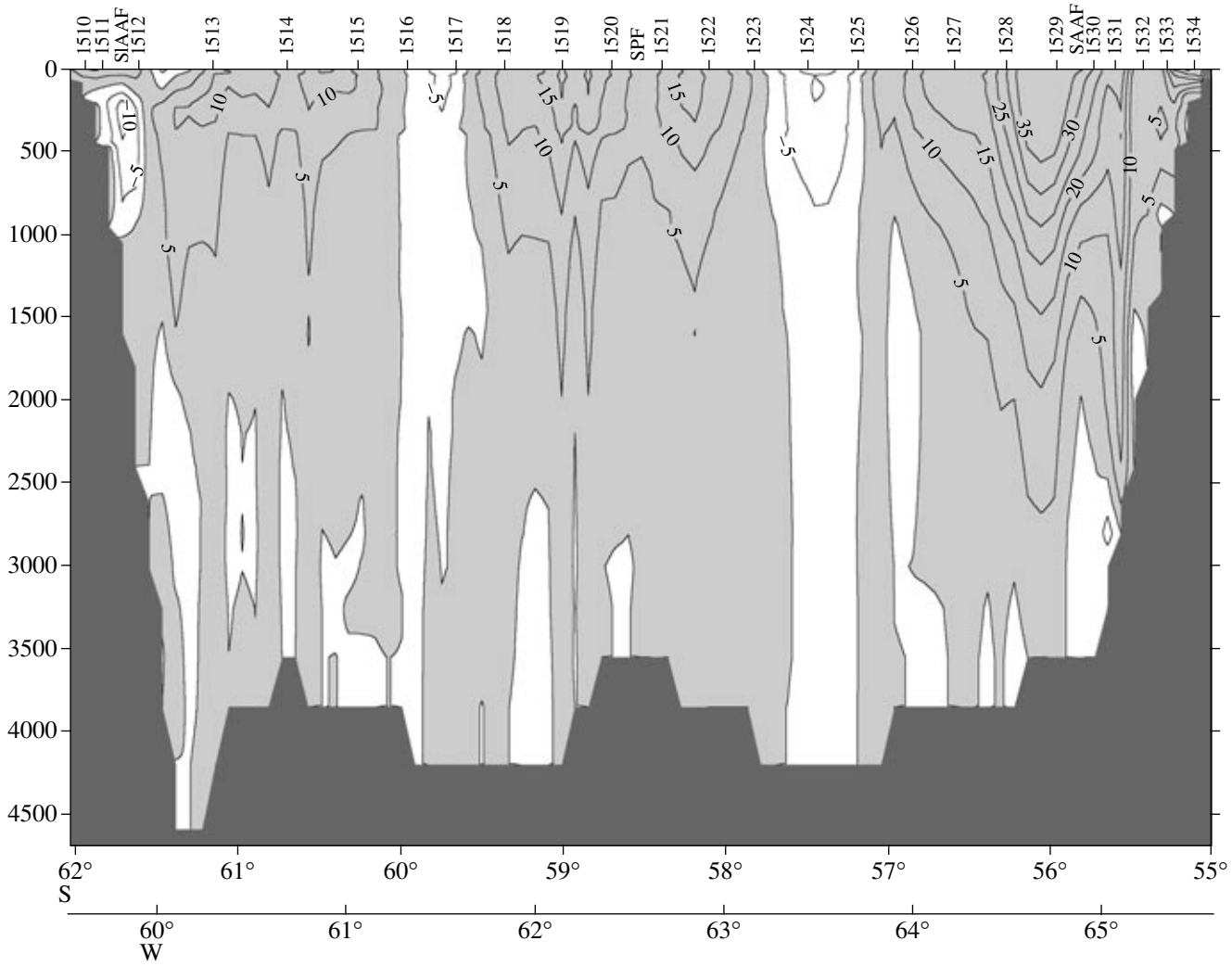

Fig. 8. Velocities at the ocean bottom. See Fig. 5 for other notations.

August and a minimum in January. The mean value of the transport in December 1979 was equal to 122×10^6 m^3/s. Thus, there is full coincidence of the estimates of the integral transport obtained as a result of our calculations with the data of the observations in December 2003 and the measurements in 1979–1980. It is possible that this points to a small interannual variability of the integral water transport via the Drake Passage.

It was noted in the Introduction that the assumption about a zero velocity of the near-bottom current in the Drake Passage leads to significant errors both in the pattern of the currents considered and in the estimate of the water transport via the strait. As an illustration of this statement, the distribution of the velocity component of the current normal to the section obtained from the calculated distribution (Fig. 5) by subtracting the near-bottom velocity from the velocity values at all the depths over this vertical is shown in Fig. 8. The integral transport via the strait corresponding to Fig. 8 is equal to 89.8×10^6 m^3/s. From a comparison of Figs. 5 and 8, it follows that the artificial assumption that the velocity at the bottom is zero not only reduces the estimate of the transport by more than a quarter but also significantly distorts the vertical structure of the currents.

CONCLUSIONS

(1) The calculation of the currents in the Drake Passage on the basis of the data of the hydrophysical section occupied in December 2003, as well as by the altimetric and other data, reveals a classical structure of the current field with three jets of the ACC: the Sub-Antarctic Current (SAAC), the South Polar Current (SPC), the Southern Antarctic Current (SthAAC), and the westerly Slope Antarctic Current (SlAAC). The transports by the SAAC, the SPC, and the SthAAC appeared close.

(2) Under the SAAC, a deep countercurrent was obtained, which agrees with the data of direct measurements of the currents in 1975.

(3) It was found that the formation of cold cyclonic eddies due to the separation of cyclonic meanders from the current is characteristic not only of the SAAC and the SPC but also of the SthAAC.

(4) It was supposed that, during the period of the observations, the water that composed the upper part of the SlAAC was formed in the Bransfield Strait and was transported to the Drake Passage via the Loper Strait between King George and Elephant islands.

(5) The integral water transport via the Drake Passage, which was equal to 122×10^6 m^3/s, appeared exactly equal to the integral transport in December 1979, which possibly points to a comparatively low interannual variability of this parameter of the currents.

(6) It was confirmed that the calculations of the currents in the Drake Passage, assuming that the geostrophic near-velocity is zero, significantly distort the real structure of the water transport via the strait.

ACKNOWLEDGMENTS

The authors are grateful to V.B. Zalesnyi for useful comments. This study was supported by the Russian Foundation for Basic Research (project no. 06-05-6420), the Program of Basic Research of the Presidium of the RAS, the "World Ocean" Federal Targeted Program of the Russian Federation, the Frontier Research System for Global Change, JAMSTEC (Japan), and by the International Arctic Research Center (Fairbanks, USA).

REFERENCES

1. V. A. Burkov, "Antarctic Jets," Okeanologiya **34** (2), 169–177 (1994).
2. M. N. Koshlyakov and R. Yu. Tarakanov, "Antarctic Circumpolar Water in the Southern part of the Pacific Ocean," Okeanologiya **43** (5), 607–621 (2003) [Oceanology **43** (5), 607–621 (2003)].
3. E. G. Morozov, A. V. Sokov, S. S. Lappo, et al., "Variability of the Discharges of the Antarctic Circumpolar Current and the Position of Frontal Zones in the Drake Passage," Dokl. Akad. Nauk **400** (6), 813–817 (2005).
4. D. A. Nechaev, G. G. Panteleev, and M. I. Yaremchuk, "Reconstruction of the Circulation in Limited Regions of an Ocean with Open Boundaries: Climatic Circulation in the Tsusima Strait," Okeanologiya **45** (6), 805–825 (2005) [Oceanology **45** (6), 761–780 (2005)].
5. H. L. Bryden and R. D. Pillsbury, "Variability of Deep Flow in the Drake Passage from Year-Long Current Measurements," J. Phys. Oceanogr. **7** (6) 803–810 (1977).
6. S. A. Cunningham, S. G. Alderson, B. A. King, et al., "Transport and Variability of the Antarctic Circumpolar Current in Drake Passage," J. Geophys. Res. **108** (C5), 8084 (2003) [doi: 10.1029/2001JC001147].
7. N. Ducet and P. Y. Le Traon, "Global High-Resolution Mapping of Ocean Circulation from TOPEX/Poseidon and ERS-1 and -2," J. Geophys. Res. **105** (C8), 19477–19498 (2000).
8. M. A. Garcia, I. Blade, A. Cruzado, et al., "Observed Variability of Water Properties and Transports on the World Ocean Circulation Experiment SR1b Section across the Antarctic Circumpolar Current," J. Geophys. Res. **107** (C10), 3162 (2002) [doi: 10.1029/2001JC000277].
9. O. Lopez, M. A. Garcia, D. Gomis, et al., "Hydrographic and Hydrodynamic Characteristics of the Eastern Basin of the Bransfield Strait (Antarctica)," Deep-Sea Res. I. **46**, 1755–1778 (1999).
10. G. Madec, P. Delecluse, V. Imbard, et al., *OPA 8.1 Ocean General Circulation Model. Reference Manual. Note du Pole de Modelisation* (Institute Pierre–Simon Laplace (IPSL), France, 1999).
11. A. C. Naveira Garabato, E. L. McDonagh, D. P. Stevens, et al., "On the Export of Antarctic Bottom Water from the Weddell Sea," Deep-Sea Res. II [ITAL] **49**, 4715–4742 (2002).
12. W. D. Nowlin, T. Whitworth, and R. D. Pillsbury, "Structure and Transport of the Antarctic Circumpolar Current at Drake Passage from Short-Term Measurements," J. Phys. Oceanogr. **7** (11), 788–802 (1977).
13. W. D. Nowlin and W. Zenk, "Westward Bottom Currents along the Margin of the South Shetland Island Arc," Deep-Sea Res. I **35** (2), 269–301 (1988).
14. A. H. Orsi, T. Whitworth, and W. D. Nowlin, "On the Meridional Extent and Fronts of the Antarctic Circumpolar Current," Deep-Sea Res. I **42** (5), 641–673 (1995).
15. H. A. Sievers and W. J. Emery, "Variability of the Antarctic Polar Frontal Zone in the Drake Passage—Summer 1976–1977," J. Geophys. Res. **83** (C6), 3010–3022 (1978).
16. H. A. Sievers and W. D. Nowlin, "Upper Ocean Characteristics in Drake Passage and Adjoining Areas of the Southern Ocean, 39°W–95°W," in *Antarctic and Resources Variability*, Ed. by D. Sahrhage (Springer, Berlin, 1988), pp. 57–80.
17. J. Sprintall, "Seasonal to Interannual Upper-Ocean Variability in the Drake Passage," J. Mar. Res. **61** (1), 27–57 (2003).
18. M. Visbeck, "Deep Velocity Profiling Using Lowered Acoustic Doppler Current Profiler: Bottom Track and Inverse Solution," J. Atmosph. Oceanic Technol. **19** (5), 794–807 (2002).
19. T. Whitworth, W. D. Nowlin, A. H. Orsi, et al., "Weddell Sea Shelf Water in the Bransfield Strait and Weddell–Scotia Confluence," Deep-Sea Res. I **41** (4), 629–641 (1994).
20. T. Whitworth, W. D. Nowlin, and S. J. Worley, "The Net Transport of the Antarctic Circumpolar Current through Drake Passage," J. Phys. Oceanogr. **12** (9), 960–971 (1982).
21. T. Whitworth and R. G. Peterson, "Volume Transport of the Antarctic Circumpolar Current from Bottom Pressure Measurements," J. Phys. Oceanogr. **15** (6), 810–816 (1985).